JOURNAL OF CATALYSIS 134, 492–505 (1992)

The Effects of Structure on the Catalytic Activity and Selectivity of V_2O_5/TiO_2 for the Reduction of NO by NH_3

GREGORY T. WENT, LI-JEN LEU, RICHARD R. ROSIN, AND ALEXIS T. BELL

Center for Advanced Materials, Lawrence Berkeley Laboratory, and Department of Chemical Engineering, University of California, Berkeley, California

Received May 29, 1991; revised October 24, 1991

An investigation of the effect of catalyst structure on the activity and selectivity of TiO_2 (anatase)-supported V_2O_5 for the selective catalytic reduction of NO by NH_3 has been carried out. The structure of the catalyst and the adsorbed species present on the surface was characterized by *in situ* laser Raman spectroscopy (LRS), and the interaction of NH_3 was investigated using temperature-programmed desorption (TPD). At vanadia loadings corresponding to less than a theoretical monolayer, the vanadia is present in the form of monomeric vanadyl and polymeric vanadate species. When the vanadia coverage exceeds a monolayer, crystallites of V_2O_5 form at the expense of the polymeric species. Analysis of the catalytic activity shows that the specific activity of the polymeric vanadates species is about 10 times greater than that of the monomeric vanadyl species. Monomeric species produce N_2 as the principle reaction product, independent of the presence or absence of O_2 in the feed, whereas polymeric vanadates species produce both N_2 and N_2O, with the selectivity to N_2 decreasing with increasing concentrations of O_2 in the feed. LRS experiments reveal that in the absence of O_2 in the feed stream, the catalyst undergoes reduction but that in the presence of O_2, the catalyst remains in a nearly fully oxidized state. TPD experiments indicate that a crucial step in the catalytic reduction of NO is the activation of adsorbed NH_3 to produce NH_x ($x = 0 - 2$) species. The removal of H atoms from adsorbed NH_3 occurs via reaction with V=O groups present in clusters of monomeric vanadyl species and in polymeric vanadate species, the latter being more reactive than the former. The observations reported in this study are interpreted in terms of a reaction mechanism, which accounts for the effects of catalyst structure and oxidation state on the observed properties.

INTRODUCTION

Titania-supported vanadia is a highly active catalyst for the selective catalytic reduction of NO by NH_3 in the presence of O_2 (*1*). Previous research has shown that the preferred phase of TiO_2 is anatase (*2–4*) and that the activity per gram of catalysts increases with increasing vanadia loading up to the point where the surface of the support is covered by a theoretical monolayer of vanadia (*2–5*). Spectroscopic studies of submonolayer coverages of vanadia on TiO_2 have shown that the dispersed vanadia is present as a combination of monomeric vanadyl and polymeric vanadate species (*6–11*), with the distribution of these two structures varying with the loading of vanadia (*11*). When the vanadia loading is raised above the dispersive capacity of the support, crystallites of V_2O_5 are observed (*5, 8–12*), and the activity of the catalyst declines (*2, 3, 5*). For a fixed vanadia loading, the activity has been found to increase upon addition of O_2 to the gas phase (*2, 4, 13–16*). IR, XPS, and ESR studies suggest that the role of O_2 is to maintain the vanadia in a highly oxidized state (*4, 13, 16*). Efforts to explain the mechanism of NO reduction by NH_3 have been made on the basis of isotopic tracer experiments (*17–20*) and spectroscopic studies of the stable adsorbed species (*13, 16, 21–24*). Using mixtures of $^{15}NH_3$ and ^{14}NO, it has been observed that $^{15}N^{14}N$ and $^{15}N^{14}NO$ are produced selectively, suggesting that the reduction of NO occurs via reaction of NO with an NH_x species on the catalyst surface (*13, 15–24*). The

0021-9517/92 $3.00

reactive NH_x species proposed by these authors varies from $x = 2$ (*16, 18–20, 22*) to $x = 4$ (*13, 17, 21, 23*).

The objective of the present study is to establish the relative activities and selectivities of the different forms of vanadia dispersed on titania and the effect of O_2 on their catalytic properties. The structure of the catalyst under reaction conditions is characterized using laser Raman spectroscopy (LRS). Temperature-programmed desorption (TPD) is used to probe the interaction of adsorbed NH_3 with the catalyst surface. The oxidation state of the catalyst following the reaction is estimated using temperature-programmed oxidation (TPO). The results obtained using these techniques are discussed in the light of a proposed reaction mechanism.

EXPERIMENTAL

The preparation of the catalysts used in this study is described elsewhere (*25*). The anatase phase of titania, referred to as TiO_2(a), was prepared by the slow hydrolysis of titanium isopropoxide (DuPont Tyzar) in water at 268 K. The resulting solution was washed with deionized water, dried for 24 h at 383 K, then calcined for 6 h at 773 K in oxygen. The phase of the titania, determined by X-ray diffraction and Raman spectroscopy, was found to be ~95% anatase and ~5% brookite. Vanadium was introduced by incipient wetness impregnation of the support with a vanadium oxalate solution. After impregnation, the materials were dried at 473 K for 2 h, then calcined in pure O_2 at 773 K for 4 h. Vanadia weight loadings were determined using X-ray fluorescence. The BET surface area was determined by N_2 adsorption at 77 K.

The gases used in this study were helium (Matheson High Purity Grade, 99.995%), oxygen (Matheson Grade, 99.99%), nitrogen (Matheson High Purity Grade 99.998%), 1.07% NH_3/He (Matheson Custom Grade), 1.0% O_2/He (Matheson Custom Grade), 4.95% NH_3/He (Matheson Custom Grade), and 2.0% NO/He (Matheson Custom Grade).

The catalytic activity of each sample was determined in a recycle reactor operated at a recycle ratio of 200 (*26*). Catalysts were pelletized, crushed, and sieved to between 30 and 60 mesh before loading onto a porous quartz frit inside the quartz reactor. The loading of vanadium in the reactor was fixed at 17 μmol, and the total sample weight ranged from 0.030 to 0.460 g. Prior to reaction, the catalyst was calcined in flowing O_2 at 773 K for 1 h. After cooling to the desired temperature, the feed consisting of 0.5% NH_3, 0.5% NO, and 0–0.5% O_2 in a balance of He was introduced. The total feed flow rate was 100 cm^3/min. The concentrations of NH_3, NO, and N_2O in the feed and exit streams were determined by Fourier-transform infrared spectroscopy and the concentration of N_2 was determined using a dual-column gas chromatograph (*26*). No NO_2 was observed in the course of the present experiments. Nitrogen balances were closed to within ±5% when O_2 was absent from the feed. When O_2 was present in the effluent, a reaction in the GC column between NO and O_2 forming N_2 made analysis of N_2 difficult. In such cases, N_2 concentrations were calculated by difference.

TPD and TPO experiments were carried out in a quartz microreactor connected to a flow manifold. The effluent was analyzed by a quadrupole mass spectrometer (UTI Model 100C). Catalyst particles between 30 and 60 mesh were loaded onto a porous quartz frit inside the quartz reactor. A constant vanadium loading of 50 μmol was maintained in the reactor. Prior to the start of a TPD experiment, the sample was heated in O_2 at 773 K for 1 h and then cooled to the desired adsorption temperature. After repeated pump–purge cycles in He, to reduce the O_2 mass spectrometer signal to background levels, a 0.5% NH_3/He stream was passed through to the reactor for 0.5 h. A 1-h He purge followed the adsorption, after which the sample was ramped to 773 K at 20 K/min in 50 cm^3/min of flowing He. During a TPD experiment, up to 20 masses were followed at a sampling rate of 12

scans/min. Similar procedures were followed to expose the catalyst to mixtures containing NH_3/NO and $NH_3/NO/O_2$. The concentration of each component in these mixtures was 0.5%. After each TPD experiment, the sample was cooled to 298 K in He, and followed by a TPO experiment. Oxidation was carried out in a 1% O_2/He mixture fed at 20 cm^3/min. The temperature was raised at 20 K/min from 298 to 773 K and held at 773 K until the oxidation was complete.

The system used to record *in situ* Raman spectra is described in Ref. (*8*). Prior to adsorption, each sample was oxidized at 773 K for 1 h in pure O_2, cooled to the desired adsorption temperature, and then purged for 1 h in He. A flow of 100 cm^3/min of He containing NH_3, NH_3/NO, and $NH_3/NO/O_2$, with each component present at the level of 0.5%, was passed through the cell for 0.5 h. Raman spectra were excited using the 488.0-nm line of an argon ion laser (Spectra Physics Model 165) and detected using an optical multichannel analyzer (Tracor Northern Model 6134). The time required to acquire a spectrum depended on the color of the sample and ranged from 1 to 400 s for a laser power of 50 mW at the sample. Multiple scans were collected for ~1000 s. To cover the entire range from 200 to 4000 cm^{-1}, the monochromator was moved to five separate locations, and the resulting spectra merged into a single spectrum. Where necessary, the background was subtracted from the spectra using the procedure described in Ref. (*11*).

RESULTS

Catalyst Characteristics

The characteristics of the catalysts used in this study have been discussed extensively in Ref. (*11*). Table 1 summarizes the BET surface area, surface V_2O_5 fraction of each species, and the dispersion of vanadium in each sample. The structure and quantity of the monomeric and polymeric vanadia species are based on an analysis of the Raman spectra of the freshly oxidized samples (*11*). The fraction of the dispersed vanadia present as polyvanadates is 20% for the 1.3% V_2O_5/TiO_2(a) sample. As the vanadia loading increases, the polyvanadate fraction increases and reaches a maximum value of ~50% in the 6.1% V_2O_5 sample before declining due to the formation of crystallites of V_2O_5. The dispersion reported in Table 1 is defined as the number of surface vanadium atoms divided by the total vanadium loading. At loading of 6.1% and below, the dispersion of vanadium is assumed to be 1 because the vanadia is present only as monomeric vanadyls and short polymeric species (*11*). For the 9.8% loading, ~40% of the V_2O_5 is present as crystallites of V_2O_5. The surface V atoms contributed by the crystallites was estimated by assuming 30-Å cubic particles exposing the (010) planes of V_2O_5. The resulting total dispersion of 65% is in excellent agreement with measurements using O_2 chemisorption on an identically loaded catalyst, which gave a value of 68% (*8*).

TABLE 1

Catalyst Characteristics

Weight loading % V_2O_5[a]	Surface area (m^2/g)	Species fraction[b]			Dispersion[c]
		Monomer	Polymer	Crystallites	
0.0	98	—	—	—	—
1.3	79	0.80	0.20	—	1.0
3.0	78	0.67	0.33	—	1.0
6.1	44	0.52	0.48	—	1.0
9.8	28	0.33	0.29	0.38	0.65

[a] Determined by XRF to ±5%.
[b] Determined by quantitative Raman analysis (*11*).
[c] See text.

Catalytic Activity and Selectivity

Figure 1 shows a plot of the NO conversion as a function of temperature for the 1.3 and 6.1% V_2O_5/TiO_2(a) samples at various O_2 feed concentrations. Because the V_2O_5 loading in the reactor was constant, the activities of these two samples can be compared directly. It is evident from the temperature required to achieve 50% conversion

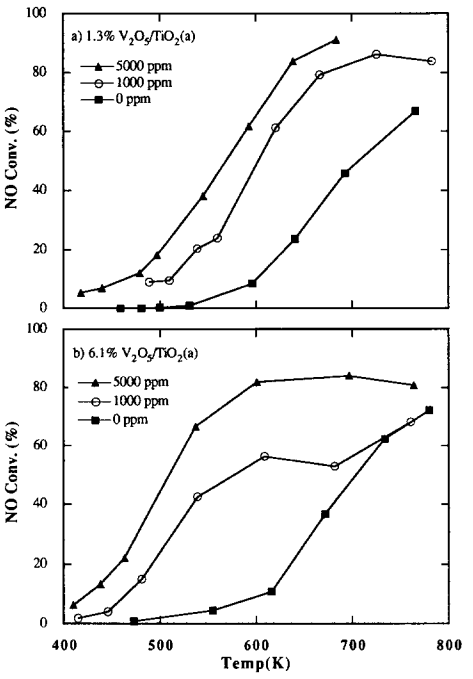

FIG. 1. NO conversion versus temperature for O_2 feed concentrations of 0, 1000, and 5000 ppm: (a) 1.3% V_2O_5/TiO_2(a) and (b) 6.1% V_2O_5/TiO_2(a).

that the 6.1% sample is more active per vanadium atom than the 1.3% sample. Gas-phase oxygen in the feed enhances the activity, and this effect is more pronounced at higher vanadia loadings. The selectivity of the catalyst, defined as the amount of N_2 formed divided by the sum of N_2 and N_2O, is shown in Fig. 2. The 1.3% V_2O_5/TiO_2(a) samples displays nearly 100% selectivity to N_2 at all temperatures and O_2 partial pressures, whereas the 6.1% V_2O_5/TiO_2(a) shows a pronounced decline in the N_2 selectivity at higher temperatures and O_2 partial pressures.

Figure 3 shows a plot of α, defined as the ratio of the moles of NO consumed divided by the moles of NH_3 consumed, as a function of temperature. In the absence of O_2 in the feed, $\alpha = 1.5$ for the stoichiometric reaction of NO and NH_3 to form N_2 and H_2O, and $\alpha = 4.0$ if N_2O is the primary product. When O_2 is added to the feed, α can decrease to 1.0, signifying that on average one N atom in N_2 and N_2O comes from NH_3 and the other from NO. Figure 3 shows that in the absence of O_2, α averages 2.5, well within the predicted range. When O_2 is present, α decreases toward unity as the temperature is raised. The decline in α with increasing temperature indicates that the participation of O_2 is activated.

The effects of vanadia loading and O_2 partial pressure on the turnover frequency (based on the number of exposed V atoms) for NO conversion at 500 K is shown in Fig. 4. The data presented in this figure correspond to an NO conversion of 10%. Application of the Weisz criterion shows that the reported results are unaffected by intraparticle mass transfer. The turnover frequency for TiO_2 (per surface Ti) is $\sim 1.0 \times 10^{-8}$ s^{-1} in the absence of O_2, and $\sim 1.0 \times 10^{-6}$ s^{-1} when the gas-phase O_2 concentration is 0.5% and, thus, can be ignored. Figure 4

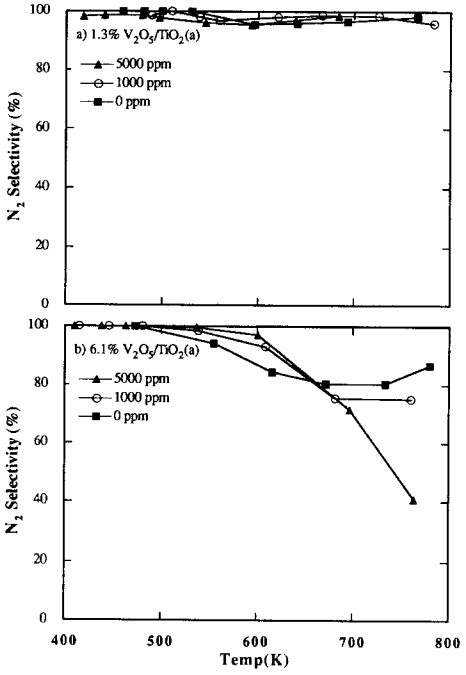

FIG. 2. N_2 selectivity, defined as $[N_2]/([N_2] + [N_2O])$, plotted versus temperature for O_2 feed concentrations of 0, 1000, and 5000 ppm: (a) 1.3% V_2O_5/TiO_2(a) and (b) 6.1% V_2O_5/TiO_2(a).

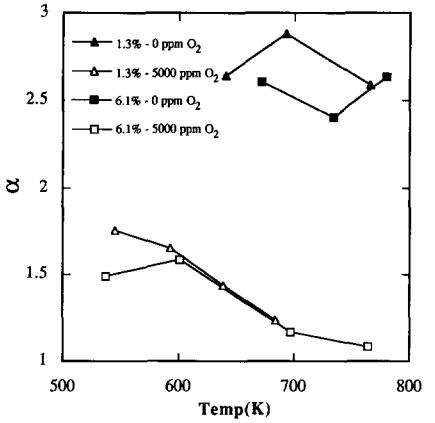

FIG. 3. A plot of α, defined as $([NO_{in}] - [NO_{out}])/([NH_{3,in}] - [NH_{3,out}])$, versus temperature for 1.3% and 6.1%/TiO_2(a) at 0 and 5000 ppm O_2 in the feed.

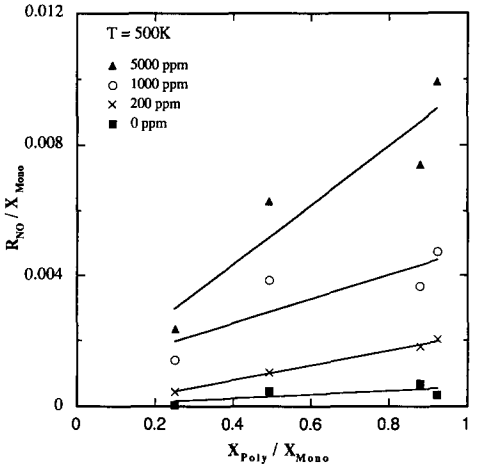

FIG. 5. A plot of R_{NO}/X_M versus X_P/X_M. Data are shown for O_2 feed concentrations of 0, 200, 1000, and 5000 ppm.

shows that the turnover frequency increases substantially with increasing V_2O_5 loading, reaching a maximum in the range of 4–8% V_2O_5. As seen in Table 1, the fraction of polyvanadate species reaches a maximum at ~6% and then declines as crystallites of V_2O_5 form at the expense of the polymeric species. This suggests that the polymeric species is more active than the monomeric species.

A simple model for the dependence of the catalytic activity on the distribution of VO_x species can be written as

$$R_{NO} = R_M X_M + R_P X_P, \qquad (1)$$

where R_{NO} is the total turnover frequency, R_M is the turnover frequency for monomeric V species, R_P is the turnover frequency for polymeric V species, X_M is the fraction of vanadium in monomeric species, and X_P is the fraction of vanadium in polymeric species. Dividing through by X_M gives

$$R_{NO}/X_M = R_M + R_P (X_P/X_M). \qquad (2)$$

A plot of R_{NO}/X_M versus X_P/X_M is displayed in Fig. 5. While the data contain significant scatter, the correlation at various O_2 partial pressures is fairly good. The ratio of R_P/R_M averages ~10 over the range of O_2 concentrations.

Figure 6 shows a plot of the N_2 selectivity as a function of the V_2O_5 loading for various O_2 concentrations in the feed. Each point on this plot corresponds to the selectivity at maximum NO conversion, which occurs between 690 and 770 K for all of the catalysts studied. It is evident that the N_2 selectivity decreases monotonically with increasing vanadia loading and that the decline in selectivity becomes increasingly severe with the

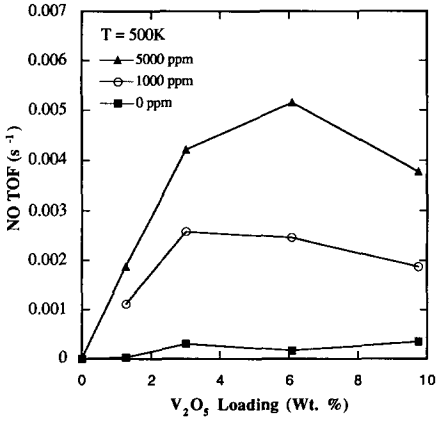

FIG. 4. The turnover frequency for NO conversion at 500 K versus V_2O_5 loading. Data are shown for O_2 feed concentrations of 0, 1000, and 5000 ppm. Estimated error of these quantities is ±10%.

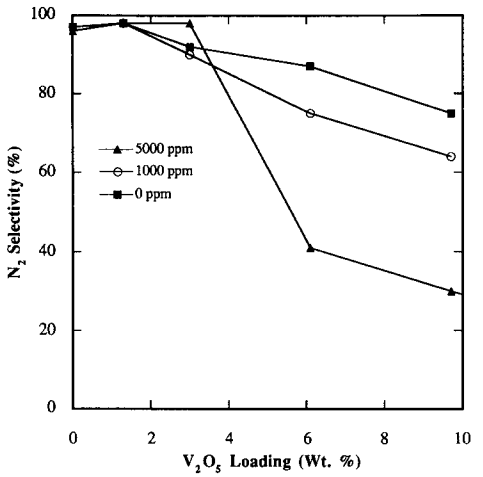

FIG. 6. N_2 selectivity at maximum conversion, defined as [N2]/([N2] + [N2O]), versus V_2O_5 loading. Data are shown for O_2 feed concentrations of 0, 1000, and 5000 ppm.

addition of O_2 to the feed. While not shown, the product of the NO/NH_3 reaction over pure V_2O_5 at 700 K is N_2O when the feed contains 0.5% oxygen.

Temperature-Programmed Desorption and Oxidation

Figures 7–9 show the TPD profiles observed following exposure of the catalysts for 0.5 h at 373 K to mixtures containing NH_3, NO, and O_2. The main purpose of these experiments is to examine the effects of NO and O_2 on the distribution of products formed during desorption of NH_3. For TiO_2(a) and 1.3% V_2O_5/TiO_2(a), the TPD profiles in Figs. 7 and 8 following exposure to NH_3 exhibit a strong desorption peak for NH_3, as well as smaller peaks for H_2O, N_2, NO, and N_2O. These latter species are formed by decomposition of NH_3, the catalyst serving as the source of oxygen for H_2O, N_2O, and NO. The addition of NO to the adsorbing mixture has no noticeable effect on these profiles, but the addition of NO and O_2 has a dramatic effect. In the case of TiO_2(a), large quantities of N_2, NO, and N_2O are seen to desorb at 660 K. Similar effects are observed for the 1.3% sample, but the peak temperatures for N_2, NO,and N_2O are shifted to 600 K. As shown in Fig. 9, NH_3 adsorption on the 6.1% sample results in the evolution of significant amounts of N_2, NO, and N_2O at 550–575 K. The addition of NO (not shown) shifts all of the TPD peaks to slightly higher temperatures, whereas the addition of NO and O_2 returns the peaks to the temperatures observed after NH_3 adsorption alone.

Further information regarding the effects of NO and O_2 on the adsorption and decomposition of NH_3 is obtained from the integrals of the TPD profiles shown in Figs. 7–9. Figure 10a shows the ratio of the amount of NH_3 adsorbed from NH_3/He mixtures containing NO or NO and O_2 to the amount of NH_3 adsorbed in the absence of NO and O_2, for an adsorption temperature of 373 K. It

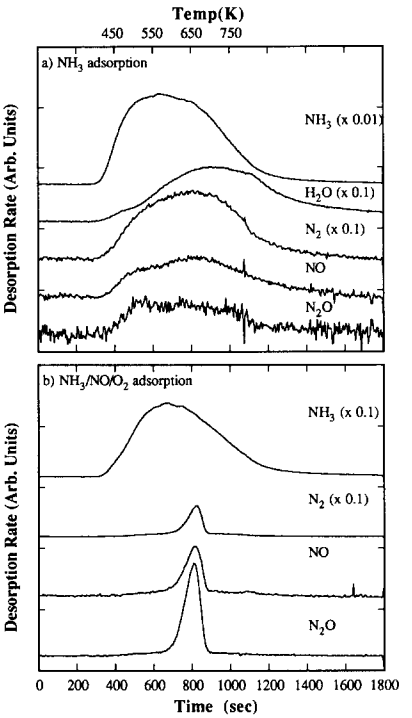

FIG. 7. TPD profiles following exposure for 0.5 h at 373 K of TiO_2(a) to mixtures containing 0.5% NH_3 (a) and $NH_3/NO/O_2$ (b). The lower axis corresponds to time, the upper axis is the temperature change during the ramp from 373 to 773 K at 30 K/min, starting at $t \sim 300$ s.

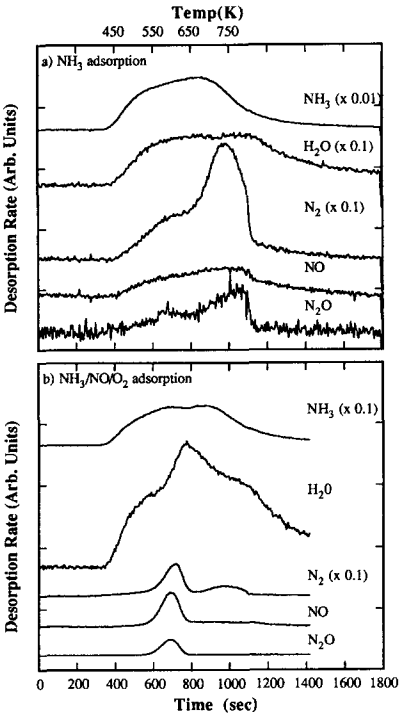

FIG. 8. TPD profiles following exposure for 0.5 h at 373 K of the 1.3% V_2O_5/TiO_2(a) sample to mixtures containing 0.5% NH_3 (a) and $NH_3/NO/O_2$ (b). The lower axis corresponds to time, the upper axis is the temperature change during the ramp from 373 to 773 K at 30 K/min, starting at $t \sim 300$ s.

is evident that the addition of NO and O_2 does not greatly affect the inventory of nitrogen on the surface. The plots in Figs. 10b and 10c report the fraction of nitrogen-containing products that desorb as N_2, NO, and N_2O and the fraction of NO_x (i.e., NO and N_2O), respectively. In both cases, the addition of NO does not perturb the product distribution, whereas the addition of NO and O_2 causes a substantial increase in the fraction of NO_x and N_2 detected.

Temperature-programmed oxidation was used to obtain an estimate of the oxidation state of the catalyst under reaction conditions. These experiments were carried out in the following manner. Gas mixtures containing 0.5% concentrations of NH_3, or NH_3 and NO, or NH_3, NO, and O_2 were passed over the catalysts for 0.5 h. All of the adsorbed species were removed by TPD, after which the sample was cooled and reoxidized by TPO. Figure 11 is a plot of the total oxygen uptake during TPO as function of the vanadia loading for a reaction temperature of 673 K. It is evident that the greatest uptake of O_2 occurs upon exposure of the catalyst to NH_3 alone and that the uptake of O_2 decreases when a mixture of NH_3 and NO, or NH_3, NO, and O_2 is passed over the catalyst. The average oxidation state of vanadium prior to TPO can be estimated from the amount of O_2 consumed during TPO, assuming that the final oxidation state of vanadium is +5. On this basis, the oxidation state of the 6.1% sample is +3.6 when exposed to NH_3 alone, +4.1 when exposed to a NH_3/NO mixture, and +4.6 when exposed to a $NH_3/NO/O_2$ mixture. It should

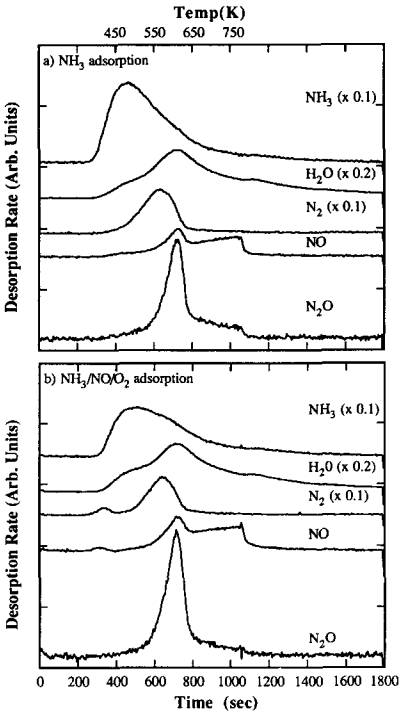

FIG. 9. TPD profiles following exposure for 0.5 h at 373 K of the 6.1% V_2O_5/TiO_2(a) sample to mixtures containing 0.5% NH_3 (a) and $NH_3/NO/O_2$ (b). The lower axis corresponds to time, the upper axis is the temperature change during the ramp from 373 to 773 K at 30 K/min, starting at $t \sim 300$ s.

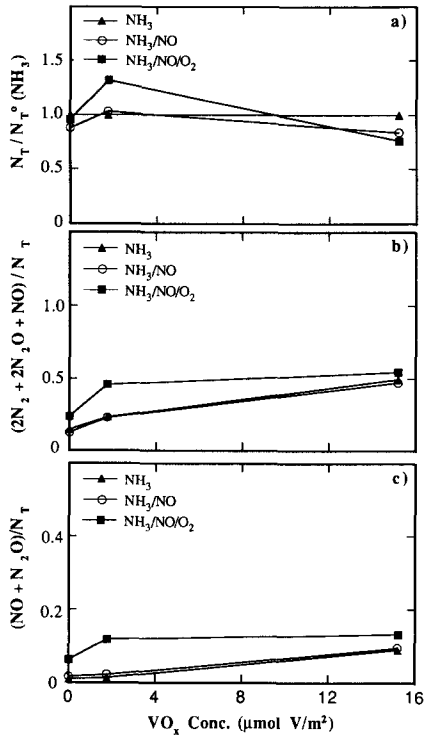

FIG. 10. The dependence on V_2O_5 loading of (a) the amount of NH_3 adsorbed from mixtures containing NO and NO plus O_2 relative to the amount of NH_3 adsorbed in the absence of NO and O_2; (b) the fraction of the nitrogen-containing products which desorb as N_2, N_2O, and NO; and (c) the fraction of nitrogen-containing products which desorb as NO and N_2O. The data shown are obtained by integration of the TPD profiles produced following NH_3 adsorption at 373 K. N_T^0 is the amount of NH_3 adsorbed in the absence of NO and O_2, and N_T is the amount adsorbed in the presence of NO and O_2.

be noted, however, that these figures represent a lower limit on the oxidation state of the catalyst under reaction conditions, since a certain amount of oxygen is removed from the catalyst during TPD. For the conditions reported in Fig. 10, this correction to the uptakes is less than 2%.

Raman Spectroscopy

In situ Raman spectra were taken during exposure of the catalysts to mixtures containing NH_3, NH_3, and NO, and NH_3, NO, and O_2. The purpose of these experiments was to identify the adsorbed species present on the catalyst surface and to assess changes in the catalyst structure caused by the interaction of the gas-phase components with the catalyst. The temperatures and gas mixtures used for these experiments were identical to those used for the TPD/TPO experiments reported in Figs. 7–11.

Figure 12 shows *in situ* Raman spectra taken at 373 and 673 K for TiO_2(a). The spectrum observed during exposure of the sample to NH_3 at 373 K exhibits peaks at 3394, 3265, and 3159 cm^{-1} due to the ν_3, ν_1, and $2\nu_4$ modes of NH_3 chemisorbed at Lewis acid sites on the TiO_2(a) surface (*22–24, 29–32*). The band located at 3315 cm^{-1} is assignable to the ν_1 mode of physisorbed NH_3 and the band at 3350 cm^{-1} to NH_x(x = 1 or 2) species produced by the dissociative adsorption of NH_3 (*29*). The bands at 3665 and 3675 cm^{-1} are due to OH groups on the TiO_2(a) (*29–32*). The increase in the intensity of these features can be ascribed to the formation of additional OH species as a consequence of NH_3 dissociation. The addition of NO or NO and O_2 to the mixture does not perturb the position of any of the above mentioned bands. A slight increase in the

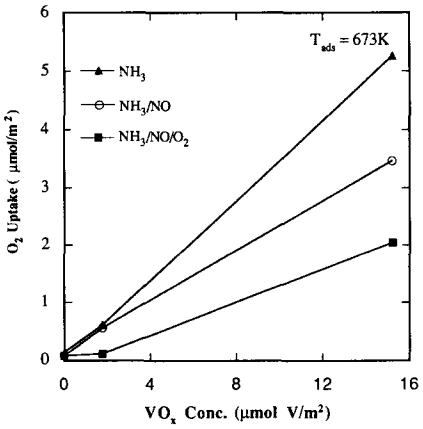

FIG. 11. Total O_2 uptake determined from integrated TPO profiles obtained following 0.5 h exposure of each catalyst at 673 K to a gas mixture containing 0.5% NH_3, 0.5% NH_3/NO, and 0.5% NH_3/NO/O_2. Adsorbed species were removed from the catalyst surface by TPD.

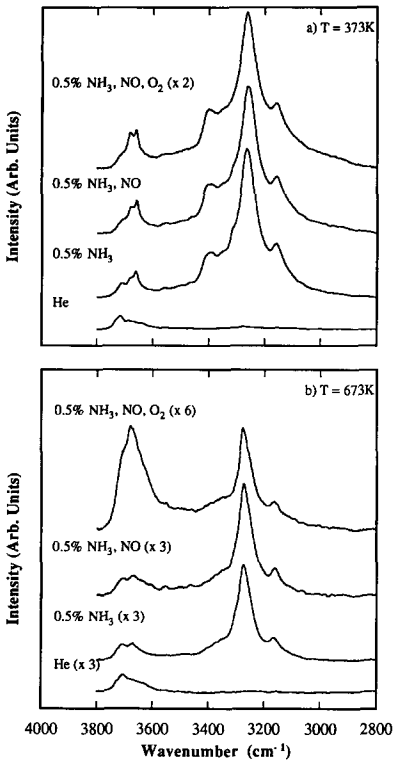

FIG. 12. *In situ* Raman spectra of TiO_2(a), recorded at 373 K (a) and 673 K (b) in the atmospheres listed by each spectrum. Spectra are displayed following subtraction of a linear background over the region of 2800–3800 cm^{-1}.

intensity of the OH band at 3665 and 3675 cm^{-1}, as well as the NH_x band at 3350 cm^{-1}, indicates that the presence of NO and O_2 increases the extent of NH_3 dissociation. No evidence for adsorbed NO was found, either in the absence or presence of O_2.

Raising the adsorption temperature to 673 K has a pronounced effect on the Raman spectra of NH_3 adsorbed on TiO_2(a), as shown in Fig. 12b. The presence of NO or NO and O_2 causes a decline in the intensity of the NH_3, and an increase in the relative intensity of bands due to OH groups, particularly when O_2 is present in the gas phase. As was the case at 373 K, no evidence for adsorbed NO was found at 673 K.

In situ Raman spectra of the 1.3% V_2O_5/TiO_2(a) and 6.1% V_2O_5/TiO_2(a) samples are shown in Figs. 13–15. Bands associated with adsorbed NH_3 are observed at 3265 and 3180 cm^{-1} in the spectra recorded following exposure of the 1.3% sample to NH_3 at 373 K (Fig. 13a). The location of the ν_1 mode is identical to that seen on TiO_2(a) (Fig. 12); however, the $2\nu_4$ band at 3180 cm^{-1} is shifted by +21 cm^{-1} from its location on TiO_2(a), evidence for a slight perturbation of the adsorbed NH_3 by the dispersed VO_x species (*24*). The addition of NO or NO and O_2 to NH_3 has no effect on the position of the bands associated with adsorbed NH_3. Figure 13b shows that exposure of the 1.3% V_2O_5/TiO_2(a) to NH_3 shifts the location of the monomeric vanadyl stretch from 1030 to

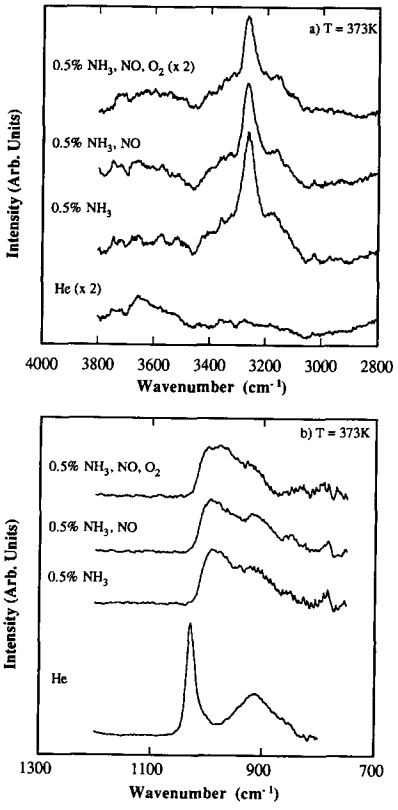

FIG. 13. *In situ* Raman spectra of 1.3% V_2O_5/TiO_2(a) recorded at 373 K in the atmospheres listed by each spectrum. Spectra are displayed over two regions: (a) 2800–3800 cm^{-1}, following subtraction of a linear background and (b) 700–1300 cm^{-1}, following subtraction of the TiO_2(a) background.

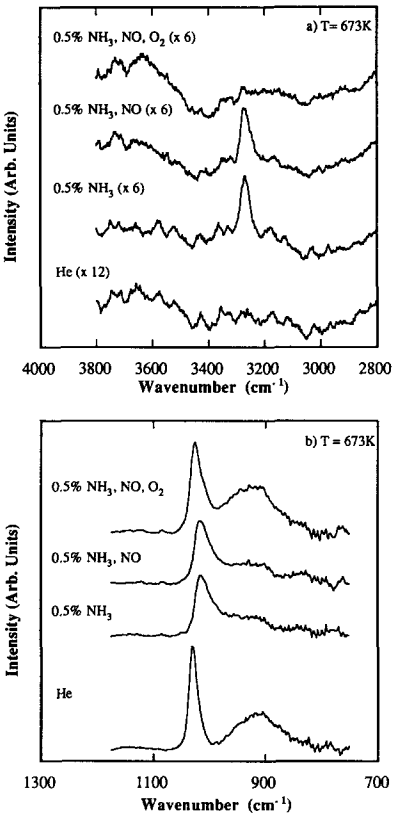

FIG. 14. *In situ* Raman spectra of 1.3% V_2O_5/TiO_2(a) recorded at 673 K in the atmospheres listed by each spectrum at 673 K. Spectra are displayed over two regions: (a) 2800–3800 cm^{-1}, following subtraction of a linear background and (b) 700–1300 cm^{-1}, following subtraction of the TiO_2(a) background.

990 cm^{-1}. This perturbation is attributable to the coordination of NH_3 to the monomeric species (*22–24*). On the other hand, the lack of change in the 915 cm^{-1} peak suggests that NH_3 does not greatly affect the polyvanadate sepcies in this sample. The presence of NO and O_2 in the gas phase also has no effect on the Raman bands arising from dispersed VO_x species.

NH_3 adsorption on the 1.3% V_2O_5/TiO_2(a) sample is less extensive at 673 K than at 373 K, as evidenced by the decrease in intensity of Raman bands for N—H stretching vibrations, shown in Fig. 14a. As was the case at 373 K, the addition of NO to NH_3 in the gas phase has no effect on the position or intensities of the peaks in the N–H stretching region of the spectra. When O_2 is added to the gas phase, the peaks for adsorbed NH_3 disappear, most likely due to the lower concentration of NH_3 in the gas phase caused by the rapid consumption of NH_3 in the reduction of NO.

The effect of gas-phase composition on the structure of dispersed VO_x species at 673 K is shown in Fig. 14b. Consistent with the lower extent of adsorption at the higher temperature, the shift in the position of the V=O band associated with the monomeric vanadyl species is less at 673 K than at 373 K. The intensity of the band at 915 cm^{-1} associated with polymeric vanadate species is much lower at 673 K due to the partial reduction of these species by NH_3 (24). When NH_3 and NO are present in the gas phase, no change is observed in the polymeric or monomeric species. However, when O_2 is introduced with the NH_3 and NO, the intensity of the band at 915 cm^{-1} due to dioxo V=O groups of the polyvanadate species increases and the peak due to the monomeric species shifts to higher wavenumber. These changes are indicative of a reoxidation of the polyvanadate species and a decrease in the degree of coordination of NH_3 with the monomeric species.

Figure 15 illustrates the effect of gas-phase composition on the structure of 6.1% V_2O_5/TiO_2(a). Due to intense absorption of incident radiation by the sample, peaks could not be observed in the region from 2800 to 3800 cm^{-1}. At 373 K, the spectrum in Fig. 15a shows that the adsorption of NH_3 causes a shift to lower energy of the peak at 1030 cm^{-1} attributed to monomeric vanadyl groups, as well as the peak at 960 cm^{-1} due to vanadyl groups in the polyvanadate species. For the monomeric species, the down scale shift is attributed to the coordination of NH_3 to this species while for the polymeric species, a much larger shift is seen, consistent with the formation of V–OH groups (*24*). The broad peak located at 955 cm^{-1} due to the dioxo-groups in the polymeric species is not perturbed by the adsorbing

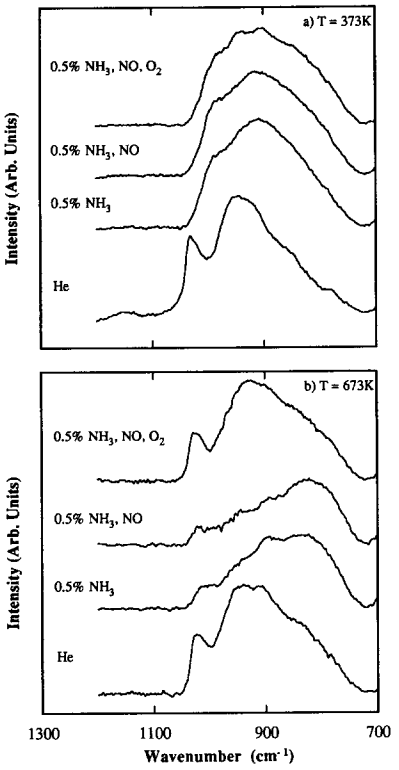

FIG. 15. *In situ* Raman spectra of 6.1% V_2O_5/TiO_2(a), recorded at 373 K (a) and 673 K (b) in the atmospheres listed by each spectrum. Spectra are displayed following subtraction of the TiO_2(a) background.

NH_3, nor is the peak at 840 cm^{-1} associated with V–O–V stretches. Figure 15a also shows that the addition of NO and O_2 to NH_3 does not effect the Raman spectra recorded at 373 K. More significant changes in the structure of the polymeric VO_x species are seen in the spectra recorded at 673 K. Upon exposure of the catalyst to NH_3, a significant decrease is observed in the intensity of the bands associated with terminal V=O groups in both the monomeric and polymeric species. These changes are attributable to the partial reduction of the dispersed vanadia species, due to the removal of oxygen from V=O groups (*11, 24*). The addition of NO does not influence the structure of the dispersed VO_x species very significantly. On the other hand, addition of O_2 to the NO/NH_3 mixture results in the nearly complete return of intensity to the Raman bands of the V=O groups associated with the monomeric and polymeric species. One can easily see that at 673 K, O_2 reoxidizes the VO_x species completely, given the similarity between the spectrum recorded at 673 K and that of the freshly oxidized catalyst.

DISCUSSION

The results of this investigation show that the specific activity of TiO_2-supported V_2O_5 passes through a maximum with increasing vanadia loading and that at a given loading, the activity is a strong function of the concentration of O_2 in the feed. These observations are consistent with previous studies of the effects of vanadia loading (*2–5, 15, 19*) and oxygen addition (*2, 3, 14, 15*) of SCR over V_2O_5/TiO_2 catalysts. A significant finding of the present study is that the dependence of the turnover frequency on vanadia loading can be attributed to the distribution of monomeric vanadyl and polymeric vanadate species on the catalyst surface, the polymeric species being roughly 10-fold more active than the monomeric species at 500 K. A further finding of this study is that the N_2 selectivity decreases significantly as the vanadia loading and the concentration of O_2 in the feed increase. While similar trends have been reported previously (*2, 14, 19, 33*), the present study demonstrates that the loss in N_2 selectivity coincides with the increase in the fraction of the dispersed vanadia present as polymeric species.

Both *in situ* Raman spectroscopy and TPO experiments of the catalysts following exposure to reactants reveal that when NO is reduced by NH_3 in the absence of O_2, the dispersed VO_x species undergo a partial reduction. Figure 11 shows that the extent of reduction increases with increasing temperature and decreases significantly when O_2 is added to the feed. While it has been shown previously (*11*) that in H_2, both monomeric vanadyl and polymeric vanadate species undergo reduction, the results presented here indicate that in the presence of NH_3 alone or NH_3 and NO, the terminal

V=O groups in the polyvanadates are reduced preferentially to the monomeric vanadyl species. It should be noted, though, that at vanadia loadings approaching one monolayer of TiO_2(a) (on the basis of the (010) plane of V_2O_5, i.e., > 6 wt%), Raman spectroscopy shows that the monomeric species undergo reduction as well (see Fig. 14).

The primary adsorbed species observable under reaction conditions is NH_3. Raman spectroscopy indicates that NH_3 is chemisorbed on Ti^{4+} centers associated with the support. NH_3 is also coordinated to isolated monomeric vanadyl species, as indicated by the shift of the stretching frequency of the V=O bond (*7, 8, 22–24*). It is notable, though, that the spectrum of adsorbed NH_3 is very similar in the presence or absence of dispersed VO_x species, suggesting that the N–H stretching frequencies of NH_3 attached to Ti^{4+} and V^{5+} centers are not significantly different (*22, 24*). There is also evidence from IR (*22*), Raman (*24*), and NMR (*25*) spectroscopies that NH_x(x = 1 or 2) species, formed by the dissociative adsorption of NH_3, are present on the surface of V_2O_5/TiO_2(a). Since the concentration of NH_x species is higher in the presence of dispersed vanadia than on TiO_2(a) alone, it can be inferred that the formation of these species is facilitated by the vanadia species (*22, 25*).

The absence of any spectroscopic evidence for adsorbed NO under reaction conditions is not surprising. Topsøe (*23*) has reported that NO does not adsorb on either fully oxidized V_2O_5/TiO_2 or NH_3-reduced V_2O_5/TiO_2. Though Ramis *et al.* (*22*) have seen evidence for NO adsorption at low temperatures on TiO_2(a) and V_2O_5/TiO_2(a), it is readily displaced by NH_3 under reaction conditions.

The reduction in the oxidation state of vanadium, discussed above, can be ascribed to the interaction of adsorbed NH_3 with the dispersed VO_x species. As shown in Figs. 7–10 and discussed extensively in Ref. (*24*) TPD of adsorbed NH_3 results in the appearance of NO, N_2O, and N_2 in addition to NH_3. The formation of the first three products increases in almost direct proportion to the weight loading of vanadia. It is also notable that in the absence of vanadia, nearly all of the adsorbed NH_3 desorbs as NH_3, but a small fraction decomposes to form N_2. The appearance of significant quantities of NO and N_2O as products of NH_3 TPD from V_2O_5/TiO_2 samples, but not from TiO_2(a) itself, indicates that nitrogen atoms produced by the dissociation of NH_3 can remove oxygen from vanadia, but not from TiO_2(a). Moreover, the quantity of NO plus N_2O formed increases linearly with the amount of polyvanadate species present, indicating that the O atoms in these species are more labile than those in monomeric vanadyl groups (*24*).

At 373 K, the addition of NO to NH_3 has little effect on the total inventory of nitrogen desorbing from the catalyst (see Fig. 10), from which it can be inferred that the presence of NO does not significantly affect the adsorption of NH_3. Likewise, the presence of NO during exposure of the catalyst to NH_3 has virtually no effect on the distribution of products formed. However, when the catalyst is exposed to gas mixture containing NH_3, NO, and O_2, the fraction of nitrogen-containing products appearing as NO, N_2O, and N_2 increases substantially, as does the fraction of NO plus N_2O. These results show that the presence of O_2 facilitates the decomposition of adsorbed NH_3 and the release of NO_x products.

The effects of catalyst structure and the influence of O_2 on catalyst activity and selectivity can be rationalized in terms of the following reaction mechanism:

1. $NH_{3,g} \rightleftarrows NH_{3,s}$
2. $NO_g \rightleftarrows NO_s$
3. $NH_3 + V_mO_{2.5m} \rightarrow NH_{3-x} + x/2H_2O + V_mO_{(2.5m-x/2)}$
4. $NH_{2,s} + NO_s \rightarrow N_{2,g} + H_2O_g$
5. $NH_{2,s} + NO_s + V_mO_{2.5m} \rightarrow N_2O_g + H_2O_g + V_mO_{(2.5m-1)}$
6. $NO_s + V_mO_{(2.5m-1)} \rightleftarrows N_s + V_mO_{2.5m}$
7. $1/2O_{2,g} + V_mO_{(2.5m-1)} \rightarrow V_mO_{2.5m}$.

The adsorption sites for NH_3 and NO are not specified explicitly, but the present study as well as previous work (*22–24, 29–32*) indicate that the most likely sites are Lewis acid centers associated with the TiO_2(a) (*29–32*) and the dispersed vanadyl groups (*22–24*). As discussed above, the TPD results show that the surface concentration of NH_3 is much higher than that of NO. The activation of NH_3, reaction 3, occurs when adsorbed NH_3 molecule reacts with the dispersed vanadia, represented here by $V_mO_{2.5m}$ (*m* is the number of V atoms in the species, 1–3). Activation produces NH_x species (x = 1 or 2) and unstable OH groups which rapidly react to form water (*22, 25*). The oxygen atoms participating in the activation of NH_3 are the V=O groups in either polyvanadate or densely spaced monomeric species (*24*), the former being more reactive. Previous studies on these same catalysts show that $x/2 \leq m$, since the maximum number of terminal oxygen atoms removed per vanadium in dispersed VO_x species is 1 (*11*). The formation of N_2 is shown to occur in step 4 via the reaction of NH_2 species with adsorbed NO, in agreement with a number of reported mechanisms (*16, 18–20, 22*). A similar reaction is proposed for the production of N_2O in reaction 5, but in this case, the surface must supply an additional O atom. Reactions 4 and 5 are supported by isotopic tracer studies reported by Miyamoto *et al.* (*17*) and Vogt *et al.* (*19, 20*), which show that the reaction of $^{15}NH_3$ with ^{14}NO (or $^{14}NH_3$ with ^{15}NO) produces $^{15}N^{14}N$ and $^{15}N^{14}NO$ almost exclusively when O_2 is present in the feed. The approach of α toward unity at high reaction temperatures when O_2 is present in the feed (see Fig. 3) is also consistent with the hypothesis that N_2 and N_2O are formed by reactions 4 and 5. Reoxidation of the dispersed vanadia by NO, reaction 6, is slow relative to the reduction of these species by reaction 3, as evidenced by the fact that in the absence of O_2 these catalysts are partially reduced. It is also interesting to note that isotopic tracer studies conducted with $^{18}O_2$ show that the N_2O formed is ^{18}O labeled, suggesting that the reverse of reaction 6 occurs at an appreciable rate (*18*). LRS and TPD experiments show that reoxidation by gas-phase O_2 in reaction 7 is considerably more efficient than reoxidation by NO.

The higher activity of the polyvanadate species, compared to the monomeric vanadyl species, is attributable to the greater reactivity of the V=O oxygen atoms of the polyvanadate species. When the oxygen associated with the V=O groups of the polyvanadate is not replenished rapidly, the activity of the catalyst is limited by the rate of reoxidation. Enhancement of the rate of reoxidation by the addition of O_2 restores the availability of labile surface oxygen required for the activation of NH_3. The scheme presented above also shows that the availability of labile oxygen can be increased either by increasing the surface fraction of polyvanadates or the concentration of O_2 in the feed. The observed decrease in N_2 selectivity when the supply of labile oxygen is increased can be attributed to an increase in the rate of reaction 5 relative to reaction 4.

CONCLUSIONS

The structure of V_2O_5/TiO_2(a) has a pronounced effect on the catalytic activity and selectivity for the reduction of NO by NH_3. Raman analysis of TiO_2(a)-supported V_2O_5 shows that at vanadia loadings below a monolayer, the vanadia is present as monomeric vanadyl and polymeric vanadate species. As the loading of vanadia is increased above the dispersive capacity of the support, crystallites of V_2O_5 form at the expense of the polymeric species. Analysis of the turnover frequency for NO conversion indicates that the polymeric species are approximately 10 times more active than the monomeric species, which accounts for the observed optimum in the activity versus vanadia loading. Monomeric species produce N_2 as the reaction product, irrespective of the concentration of O_2 in the feed. Polyvanadate species produce both N_2 and N_2O, with the selectivity to N_2 declining sharply

with the addition of O_2 to the feed. TPD and LRS experiments indicate that these trends are related to the activation and decomposition of NH_3 by the dispersed vanadia. This step is crucial for the reduction of NO and is accelerated by the presence of labile surface oxygen in clusters of monomeric vanadyl species and in the polyvanadate species. High concentrations of surface oxygen also lead to the production of N_2O, an undesirable by-product of the NO/NH_3 reaction. An implication of the results reported here is that V_2O_5/TiO_2(a) catalysts should be optimized by maximizing the density of the lower oligomers, preferable monomeric and dimeric vanadia species, at the exclusion of the larger polymeric species and crystallites of V_2O_5.

ACKNOWLEDGMENT

This work was supported by the Director, Office of Energy Research, Office of Basic Energy Sciences, Chemical Sciences Division of the U.S. Department of Energy under Contract No. DE-AC03-76SF00098.

REFERENCES

1. Bosch, H., and Janssen, F., *Catal. Today* **2,** 369 (1988).
2. Bauerle, G. L., Wu, S. C., and Nobe, K., *Ind. Eng. Chem Prod. Res. Dev.* **17,** 117 (1978).
3. Pearson, I. M., Ryu, H., Wong, W. C., and Nobe, K., *Ind. Eng. Chem Prod. Res. Dev.* **22,** 381 (1983).
4. Inomata, M., Miyamoto, A., Ui, T., Kobayashi, K., and Murakami, Y., *Ind. Eng. Chem Prod. Res. Dev.* **21,** 424 (1982).
5. Baiker, A., Dollenmeier, P., Glinski, M., and Reller, A., *Appl. Catal.* **35,** 351 (1989).
6. Busca, G., *Mater. Chem. Phys.* **19,** 157 (1988).
7. Cristiani, C., Forzatti, P., and Busca, G. *J. Catal.* **116,** 586 (1989).
8. Went, G. T., Oyama, S. T., and Bell, A.T. *J. Phys. Chem.* **94,** 4240 (1990).
9. Eckert, H., and Wachs, I. E., *J. Phys. Chem.* **93,** 6796 (1989).
10. Machej, T., Haber, J., Turek, A. M., and Wachs, I. E., *Appl. Catal.* **70,** 115 (1991).
11. Went, G. T., Leu, L-J., and Bell, A. T., *J. Catal.* **134,** 479 (1992).
12. Roozeboom, F., Mittelmeijer-Hazeleger, M. C., Moulijn, J. A., Medema, J., de Beer, V. H. J., and Gellings, P. J., *J. Phys. Chem.* **84,** 2783 (1980).
13. Inomata, M., Miyamoto, A., and Murakami, Y., *J. Catal.* **62,** 140 (1980).
14. Wong, W. C., and Nobe, K., *Ind. Eng. Chem Prod. Res. Dev.* **25,** 179 (1986).
15. Bosch, H., Janssen, F. J. J. G., van den Kerkhof, F. M. G., Oldenziel, J., van Ommen, J. G., and Ross, J. R. H., *Appl. Catal.* **25,** 239 (1986).
16. Odriozola, J. A., Soria, J., Somorjai, G. A., Heinemann, H., Garcia de la Banda, J. F. Lopez Granados, M., and Conesa, J. C., *J. Phys. Chem.* **95,** 240 (1991).
17. Miyamoto, A., Kobayashi, K., Inimata, M., and Murakami, Y., *J. Phys. Chem.* **86,** 2945 (1982).
18. Janssen, F. J. J. G., van den Kerkhof, F. M. G., Bosch, H., and Ross, J. R. H., *J. Phys. Chem.* **91,** 5921 (1987); **91,** 6633 (1987).
19. Vogt, E. T. C., Boot, A., van Dillen, A. J., Geus, J. W., Janssen, F. J. J. G., and van den Kerkhof, F. M. G., *J. Catal.* **114,** 313 (1988).
20. Vogt, E. T. C., van Dillen, A. J., Geus, J. W., Janssen, F. J. J. G., and van den Kerkhof, F. M. G., *J. Catal.* **119,** 270 (1988).
21. Takagi, M., Kawai, T., Soma, M., Onishi, T., and Tamaru, K., *J. Catal.,* **50,** 441 (1977).
22. Ramis, G., Busca, G., Bregani, F., and Forzatti, P., *Appl. Catal.* **64,** 259 (1990).
23. Topsøe, N.-Y., *J. Catal* **128,** 499 (1991).
24. Went, G. T., Leu, L-J., Lombardo, S. J., and Bell, A. T., *J. Phys. Chem.,* in press..
25. Went, M. S., Ph.D. thesis, Department of Chemical Engineering, University of California, Berkeley, CA, 1991.
26. Hecker, and W., Bell, A. T., *Anal. Chem.* **53,** 817 (1981).
27. Weisz, P. B., *Z. Phys. Chem.* **11,** 1 (1957).
28. Smith, J. M., "Chemical Engineering Kinetics," 3rd ed., pp. 454–467. McGraw–Hill, New York, 1981.
29. Went, G. T., and Bell, A. T., *Catal. Lett.,* **11,** 111 (1991).
30. Ramis, G., Busca, G., Bregani, F., and Forzatti, P., *Appl. Catal.* **64,** 243 (1990).
31. Busca, G., Saussey, H., Saur, O., Lavalley, J., and Lorenzelli, V. *Appl. Catal.* **14,** 245 (1985).
32. Primet, M., Pichat, P., and Mathieu, M-V., *J. Phys. Chem.* **75,** 1221 (1971).
33. Kotter, M., Lintz, H.-G., Turek, T., and Trimm, D. L., *Appl. Catal.* **52,** 225 (1989).